Synthesis of tungsten oxide nano structures by laser pyrolysis

Bonex Wakufwa Mwakikunga*

School of Physics,
University of the Witwatersrand,
Private Bag 3, PO Wits 2050,
Johannesburg, South Africa

CSIR National Centre for Nano-Structured Materials,
P.O. Box 395,
Pretoria 0001,
South Africa

Department of Physics and Biochemical Sciences,
University of Malawi,
Private Bag 303,
Chichiri, Blantyre 3, Malawi
E-mail: bmwakikunga@csir.co.za
*Corresponding author

Andrew Forbes

Council for Scientific and Industrial Research,
National Laser Centre,
P.O. Box 395,
Pretoria 0001, South Africa

School of Physics,
University of Kwazulu-Natal,
Private Bag X54001,
Durban 4000, South Africa
E-mail: aforbes1@csir.co.za

Elias Sideras-Haddad and
Rudolph Marthinus Erasmus

School of Physics,
University of the Witwatersrand,
Private Bag 3, PO Wits 2050,
Johannesburg, South Africa
E-mail: Elias.Sideras-Haddad@wits.ac.za
E-mail: Rudolph.Erasmus@wits.ac.za

Gift Katumba

Department of Physics,
University of Zimbabwe,
P.O. Box MP 167
Mt Pleasant, Harare, Zimbabwe

CSIR National Laser Centre,
P.O. Box 395,
Pretoria,
South Africa
E-mail: gkatumba@csir.co.za

Bathusile Masina

Council for Scientific and Industrial Research,
National Laser Centre,
P.O. Box 395,
Pretoria 0001, South Africa

Department of Physics,
University of Zululand,
Private Bag X1001,
Kwadlangezwa 3886, South Africa
E-mail: bmasina@csir.co.za

Abstract: Since the proposal to synthesise materials by laser assisted pyrolysis in the 1970s, and its practical realisation in 1982, a number of researchers have used this method in obtaining nano-powders from liquid droplets. This study revisits this technique by introducing a new aspect in that it considers obtaining thin films rather than powders. A full experimental arrangement, including laser optimisation, optical layout and materials processing procedures is described. Synthesis of WO_3 nanostructures by this method is reported for the first time, with the mean diameter and length determined to be 51 nm and 6.8 μm, respectively. A possible mechanism for production of such nano structures is proposed owing to the selective dissociation of the O–C bonds in the tungsten ethoxide precursor liquid which resonate with the 10.6 μm emission wavelength of the CO_2 laser employed.

Keywords: WO_3; nano-rods; laser pyrolysis; multiphoton dissociation; laser beam propagation.

Reference to this paper should be made as follows: Mwakikunga, B.W., Forbes, A., Sideras-Haddad, E., Erasmus, R.M., Katumba, G. and Masina, B. (XXXX) 'Synthesis of tungsten oxide nano structures by laser pyrolysis', *Int. J. Nanoparticles*, Vol. X, No. Y, pp.XXX–XXX.

Biographical notes: Bonex Wakufwa Mwakikunga is a Senior Lecturer in Physics in the Department of Physics and Biochemical Sciences, University of Malawi at the Polytechnic in Blantyre, Malawi. He received an MSc in Experimental Solid State Physics at the NanoScale in the University of the Witwatersrand in Johannesburg, South Africa in 2005 and presently, he is

pursuing his PhD in the same university. He is now serving as a candidate researcher at the CSIR National Centre for Nano-Structured Materials in Pretoria, South Africa.

Andrew Forbes is a Principal Researcher at the Council for Scientific and Industrial Research, National Laser Centre in Pretoria, South Africa. He also holds an Honorary Senior Lecturer position in the School of Physics, University of KwaZulu-Natal, Durban, South Africa. He received his MSc and PhD at the University of Natal (South Africa). His current research interest is in both theoretical and experimental aspects of laser beam propagation and digital holography.

Elias Sideras-Haddad is a Professor of Physics in the School of Physics at the University of the Witwatersrand in Johannesburg, South Africa. He received an MSc and a PhD in Accelerator Physics at the same University and had taken a number of Postdoctoral positions including one at Lawrence Livermore National Laboratory. His current interests are in nuclear physics, diamond physics, solid state quantum computing and cryptography and transition metal oxide nanostructures for quantum computational and information systems applications.

Rudolph Marthinus Erasmus is a Senior Research Officer in the School of Physics at the University of the Witwatersrand and is responsible for the Raman and Luminescence Laboratory. His research interests include characterisation of stress and defects in ultra-hard materials. He received an MSc in Semiconductor Physics at the University of Pretoria and is currently finalising his PhD at the University of the Witwatersrand.

Gift Katumba is a Lecturer in the Department of Physics in the University of Zimbabwe, in Harare, Zimbabwe. He received a PhD in Solid State Physics in the University of Zimbabwe in 2006 in collaboration with Uppsala University in Sweden. His work focused on selective solar absorption properties of carbon in different dielectric matrices such as ZnO, NiO and SiO_2. He is now a post-doctoral at the CSIR National Laser Centre in Pretoria, South Africa.

Bathusile Masina has completed a BSc Hons at the University of Zululand and is presently completing her MSc (University of Zululand) while working on the application of lasers to material studies of diamond at CSIR-National Laser Centre.

1 Introduction

Laser pyrolysis is based on a resonant interaction between a laser beam and a gaseous or liquid precursor (Cannon et al., 1982; Dez et al., 2004; Herlin et al., 1996; Muller et al., 2003), where energy is transferred by a multiphoton process between the emission line of the laser and at least one absorption band of the precursor. An aerosol generator produces droplets of the precursor which are carried by an inert gas (usually argon or nitrogen) into the laser beam. Multiphoton absorption by the precursor leads to dissociation; radicals are formed and the subsequent reactions result in nanoparticles by homogeneous nucleation (Haggerty and Cannon, 1981), exhibiting a narrow size distribution and high purity because the reaction takes place in an interaction zone without walls. There has been many attempts at modelling the mechanisms involved in laser pyrolysis. Bowden

et al. (1977) proposed a model for laser-induced photo-chemical reactions in which selective low-level excitation of a molecular species by the laser beam was assumed to incorporate coherent resonant energy transfer with collision damping. Other models have been specific to certain materials, for example, the simulation of CO_2 laser pyrolysis during preparation of SiC nano-powders (Amara et al., 2003; Bowden et al., 1977; El-Diasty, 2004).

In the early 1980s Haggerty and Cannon (1981) developed a laser synthesis process to produce silicon containing nanoparticles (e.g. SiC, Si_3N_4). First experiments in laser pyrolysis were reported in 1982 by Cannon et al. (1982), and since then the technique has been expanded to cover many new materials such as ceramics (van Erven et al., 1997), light-emitting Si nanoparticles (Huisken et al., 2000), fullerenes (Petcu et al., 2000; Tenegal et al., 2001), silicon-germanium alloys (Watanabe et al., 2003), Te films (Pola et al., 2004) and recently VO_2 (Mwakikunga et al., 2007).

Among several materials that can be used as active layers, tungsten oxide is highly promising. Several studies have shown that WO_3 can be used for the detection of green-house gases such as nitrogen oxides (NO and NO_2 and NO_x) (Kawasaki et al., 2002), carbon monoxides, H_2S, NH_3 and hydrocarbons such as ethanol, benzene and methane (Wang et al., 2003). WO_x electrochromism has been investigated (Leftheriotis et al., 2003) and found to be enhanced when mixed with Au and Al (Hoel et al., 2004), Ti (Sun et al., 2004; Shieh et al., 2002), Au, Pd and Pt (Ando et al., 2001) and with MoO_3 (Patil and Patil, 2001). Influence of substrate temperature (Patil et al., 2001), annealing (Jayatissa et al., 2004) and proton irradiation on the properties of WO_x have been reported (Kamal et al., 2005). Performance of WO_x has been compared with NiO_x on electrochromism (Arakaki et al., 1995), with V_2O_5 as sensitive elements for NO detection (Capanoe et al., 1999; Djerad et al., 2004) and with nano-powders of tin and indium oxides as CO and O_2 detectors (Baraton et al., 2002). However, despite the wide range of applications for WO_3, it has to date, not been synthesised using the laser pyrolysis technique.

In this paper we report on the synthesis of WO_3 nano-rods by laser pyrolysis in the far infra-red without the introduction of a flame (induced by the presence of acetylene and oxygen in other studies). In Section 2 we introduce the basic theory of laser propagation and derive expressions for the dissociation zone inside the reactor. In Section 3 the general methodology and experimental setup is presented, followed by experimental results and discussion in Section 4. The results include the production of thin films by laser pyrolysis whereas most of the few previous publications on this technique concentrated on powders. The findings are summarised in Section 5.

2 Laser dissociation zone

In this section the laser beam propagation parameters are defined and applied to determine the interaction volume of the laser beam and the precursor. A comprehensive review of laser beam definitions and laser beam propagation can be found in literature (Belanger, 1991; Siegman, 1991; Siegman and Townsend, 1993; Wright et al., 1992). We present a brief summary here to aid the reader in understanding the experimental parameters to follow.

The multimode laser beam radius $w(z)$ of the output from a stable-cavity laser is defined using the second moments of the intensity distribution $I(r,z)$. Using this

formalism, the laser beam propagation in the z direction can be described by the modified Gaussian propagation law (see Figure 1):

$$w(z) = w_0 \sqrt{1 + \left(\frac{z - z_0}{z_R} \right)^2} \tag{1}$$

where w_0 is the minimum laser beam width at position z_0, and z_R is the so-called Rayleigh range that is related to the beam quality factor M^2 and the wavelength (λ) of the laser light through the relation:

$$z_R = \frac{\pi w_0^2}{M^2 \lambda} \tag{2}$$

Figure 1 A schematic laser beam propagation after a focusing element, showing the waist and waist position

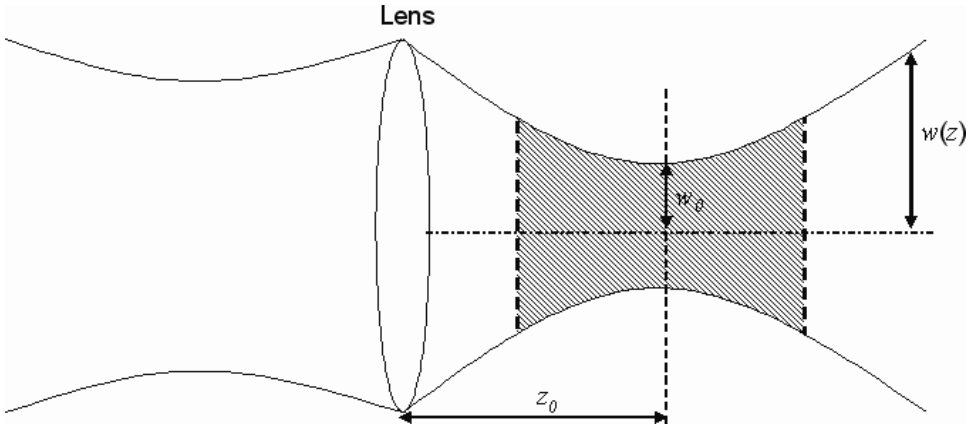

Note: The interaction volume of the laser beam with the aerosol is depicted here by the shaded area.

The Rayleigh range equals the distance at which the cross-sectional area of the laser beam doubles from the waist value and is often interpreted as a measure of how far the laser beam propagates without significant divergence. For applications where the laser beam interacts over a length rather than at a fixed plane, such as in laser pyrolysis, long Rayleigh ranges are desirable. The beam quality factor is a measure of how many modes are oscillating in the laser and impacts on the space-beam-width product:

$$w_0 \theta_0 = \frac{M^2 \lambda}{\pi} \tag{3}$$

where θ_0 is the half-angle divergence of the laser beam. Ideal Gaussian laser beams have $M^2 = 1$, while all other laser beams have $M^2 > 1$. We note that Gaussian beams will have the longest Rayleigh range of all beam types, and the smallest divergence for a given waist size. In processes such as laser pyrolysis, where long propagation

distances are desirable but with high power densities, good laser beam quality is essential.

With these parameters known, the power density $P(r,z)$ of a near Gaussian laser beam everywhere inside the reactor may be described as follows:

$$P(r,z) = \frac{2P_0}{\pi w^2(z)} \exp\left(-2\left(\frac{r}{w(z)} \right)^2 \right) \tag{4}$$

where z is the propagation distance from the final focusing element, r is the radial coordinate, and P_0 is the total power contained in the output beam. The peak power density of the laser beam is given by:

$$P_{\text{peak}}(z) = \frac{2P_0}{\pi w^2(z)} \tag{5}$$

and clearly decreases with increasing spot size, reaching a maximum at $z = z_0$. If the reactor is placed at a distance d from the final focusing element and is of length L, then the laser beam will fill a volume given by:

$$V = \int_d^{d+L} \pi w^2(z)\mathrm{d}z = \frac{\pi w_0^2 L\left(3d^2 + L^2 + 3d\left(L - 2z_0\right) - 3Lz_0 + 3\left(z_0^2 + z_R^2\right)\right.}{3z_R^2} \tag{6}$$

A special case of the aforementioned is when the interaction volume is chosen to be exactly two Rayleigh ranges; in this case the volume is given by:

$$\int_{Z_o - Z_R}^{Z_o + Z_R} \pi w^2(z)\mathrm{d}z = \frac{8\pi^2 w_0^4}{3M^2\lambda} \tag{7}$$

This analytical result is useful in getting an intuitive feel for the optimal optical delivery system: large focal spots (large w_0) will give a larger interaction volume, but the peak power density of the laser beam decreases with increasing size. If threshold power densities are required for the process, then a compromise must be made. In addition, if the process has a threshold power of P_t, then only that part of the laser beam above this threshold will be effective for dissociation, resulting in a reduced dissociation volume of:

$$V = \int_d^{d+L} \pi r_0^2(z)\mathrm{d}z \tag{8}$$

where r_0 is the radius of the 'effective' beam:

$$r_0(z) = \frac{w^2(z)}{2} \mathrm{Ln}\left(\frac{2P_0}{\pi w^2(z) P_t} \right) \tag{9}$$

The impact of laser beam parameters on such multiphoton dissociation processes has been discussed elsewhere in detail (Forbes and Botha, 2005; Forbes et al., 2002), and is beyond the scope of this paper to review. However we end this section with a brief summary of the salient points to be used in later sections: high power densities are

achieved through focusing the laser beam to reduce the beam size, but this in turn reduces the laser beam volume and Rayleigh range, thereby reducing the volume in which the precursor interacts with the laser beam. In such problems a compromise is always necessary, the extent of which is largely determined by what can be extracted from the laser in terms of laser power and beam quality.

3 Experimental methodology and setup

A six arm chamber was designed and built with adjacent arms orthogonal to one another. Two opposite arms were mounted with 2 inch ZnSe windows tilted slightly from normal incidence to avoid back reflections into the laser cavity; these formed the input and output windows for the laser beam, which propagated in the horizontal plane, parallel to the optical table, through the two-arm length. The entrance window was 145 mm from the focusing element and the total length from entrance to exit window was 590 mm. Orthogonal to the laser beam axis, in the vertically upwards direction, the precursor droplets were released into the chamber and travelled into the laser beam volume. The subsequent products were collected in one of two configurations:

1 onto a substrate for production of thin films

2 onto a filter, connected to a pump, for the production of powders.

In the thin film configuration, the substrate was mounted on a rotating stage driven by a controllable step-motor, which in turn was powered and controlled from outside the chamber via vacuum-to-atmosphere adaptors. The last pair of arms, not used in this experiment, allows for viewing the pyrolysis process through either visual or spectroscopic means. A schematic representation of the laser pyrolysis concept is shown in Figure 2.

Figure 2 An illustration of the laser pyrolysis setup (see online version for colours)

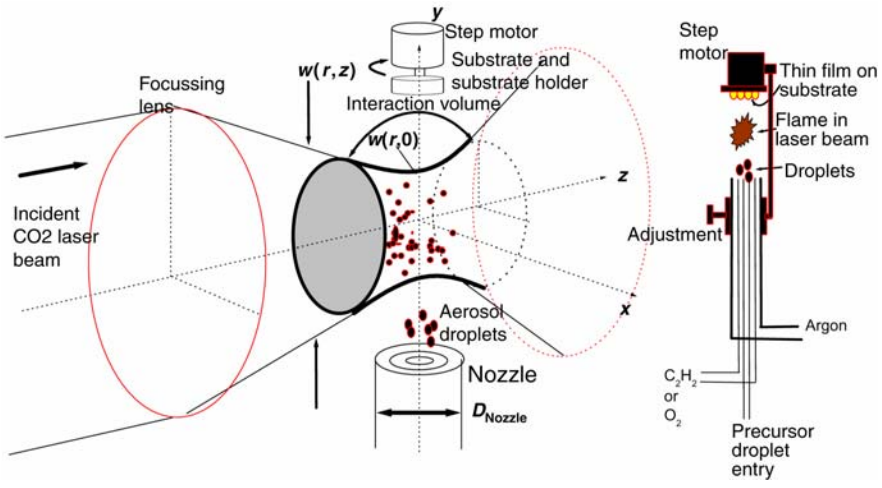

Note: The laser beam introduces a certain interaction volume into which the aerosol droplets of the precursor are released. The insert on the right illustrated the multiflow nozzle used, which allowed the separate entry of the precursor and carrier gases.

The experimental system for delivery of the laser beam is shown in Figure 3. A wavelength tuneable Continuous Wave (CW) CO_2 laser was used in the experiments (Edinburgh Instruments, model PL6). Wavelength tuneability of the laser was possible with an intra-cavity mounted grating, allowing line tuneable output in the 9.2–10.8 μm range. A pop-up mirror in the optical setup allowed the laser beam to be directed to a diagnostics table for power measurements (Coherent power meter, model 201) and for determining the lasing wavelength using a spectrum analyser (Optical Engineering Inc., model 16A). A polarisation based attenuator was used to allow power variability (this could also be achieved through adjustment of the laser discharge current). A Helium Neon laser was aligned colinear with the CO_2 beam for ease of alignment through the optical system. The laser beam was focused using a 2 m radius of curvature concave mirror (gold coated from II – VI Inc.) and the profile of the laser beam was measured at various distances from the mirror with a scanning slit to determine the complete propagation characteristics inside the reactor. Careful choice of the slit width was made for each measurement in order to ensure accurate results following the approach of Chapple (1994). Since it was clear that the intensity profile was very Gaussian-like, the beam radius at each position was calculated by using a Gaussian fit to the data. A non-linear least squares fit was used to extract the necessary laser beam parameters, such as waist, waist position and laser beam quality.

Figure 3 A schematic representation of the laser beam delivery for the synthesis of tungsten trioxide by laser pyrolysis, with the six arm pyrolysis chamber shown (two arms are in and out of the page) (see online version for colours)

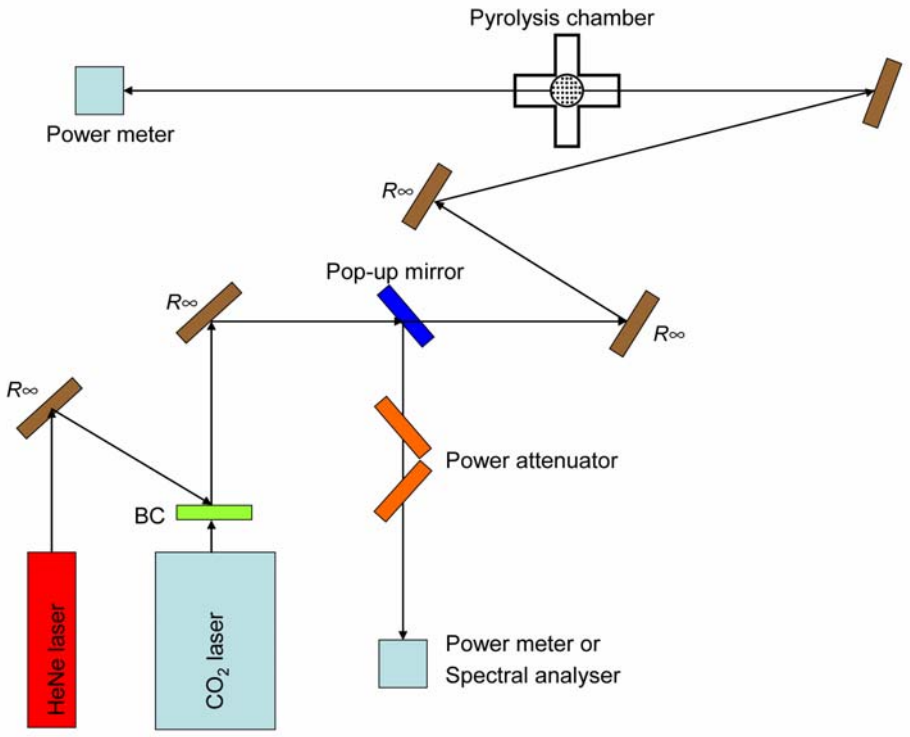

Note: The HeNe laser was used only for visible alignment of the CO_2 laser beam. The final focusing element was a 2 m curvature gold coated mirror.

The synthesis of WO_3 commenced with 5.4 mg of dark blue powder of WCl_6 (Aldrich 99.99%) dissolved in 500 ml of ethanol. Since WCl_6 is highly reactive with air and moisture, its dissolution was conducted in argon atmosphere. Optical absorption properties of the precursor were determined using a Bomem DA8 FTIR spectrometer in the wavelength range 200–4500 cm^{-1}. The precursor was decanted into a nebuliser (Microlife, model NEB 50) which was attached to the laser pyrolysis system via a multichannel nozzle (see Figure 2), allowing acetylene (C_2H_2) and/or oxygen to be included in the mix. The precursor droplets were injected into the CO_2 laser beam with an argon carrier gas. Often in such experiments a combustible combination of gases are used. In this experiment only the multiphoton dissociation route was explored, without the introduction of a flame. Particles from this process were collected on Corning glass substrates, placed on a rotating stage, at room temperature. The so-obtained samples were further annealed in argon atmosphere at 500°C for 17 hr. Morphology studies were carried out using a Jeol JSM–5600 Scanning Electron Microscopy (SEM) microscope, which was also equipped for Energy Dispersive X-ray (EDX) spectroscopy. In order to avoid charging effects during SEM analysis, the samples were made conductive by carbon coating. In order to unveil molecular composition, phonon behaviour and grain size distribution, Raman spectroscopy was carried out using a Jobin–Yvon T64000 Raman spectrograph with a 514.5 nm line from an argon ion laser. The power of the laser at the sample for Raman spectroscopy of the postannealed samples was 0.384 mW in order to minimise localised heating of the sample. The T64000 was operated in single spectrograph mode, with a 1800 lines/mm grating and a $20\times$ objective on the microscope. The experimental procedure showed good reproducibility of results.

4 Results and discussion

Experiments were performed in order to maximise both the power density of the laser beam inside the reactor and the interaction of the laser beam with the precursor. The latter requires understanding of the absorption bands of the precursor, resulting in an optimal operating wavelength, while the former requires optimising the laser output power and propagation parameters in the reactor near this desired wavelength, guided by the theoretical model described in the previous section.

The precursor's absorption characteristics were studied by infrared spectroscopy in order to determine the absorption bands that overlapped with emission lines of the CO_2 laser. The absorption spectrum of the precursor showed an absorption band around 1000 cm^{-1}, which is close to the 10P(20) (λ = 10.591 μm) laser emission line at 944 cm^{-1}, leading to the necessary dissociation. The power spectrum of the CO_2 laser was obtained in the wavelength range 9.2–10.8 μm, and is shown in Figure 4. The major bands correspond to the rotational and vibrational modes of the CO_2 molecule. In all the results that follow the laser was set to the 10P(20) line, at roughly 10.6 μm, since this had the largest power of approximately 50 W and was close to a measured absorption band of the precursor.

The laser beam was focused inside the reactor and the resulting propagation was measured. The measured data was fitted to Equation (1) and the unknown parameters w_0, z_0 and M^2 were determined. This allowed calculation of the peak power density as a function of position (from Equation (5)) and the interaction volume (from Equation (6)). The beam radius and power density as a function of position is shown in Figure 5,

with the extracted laser characteristics listed in Table 1. The laser beam was found to be near Gaussian in intensity profile, and focused to a waist diameter of roughly 2.4 mm with a maximum power density at the waist position of approximately 2.2 kW/cm^2. This ensured a volume large enough for the aerosol from the nozzle to completely interact with the laser (i.e. the entire aerosol passed through the laser beam), at roughly 4 cm^3.

Figure 4 Experimental data on the power spectrum of the laser, showing the well-known four distinct emission bands from the CO_2 laser (see online version for colours)

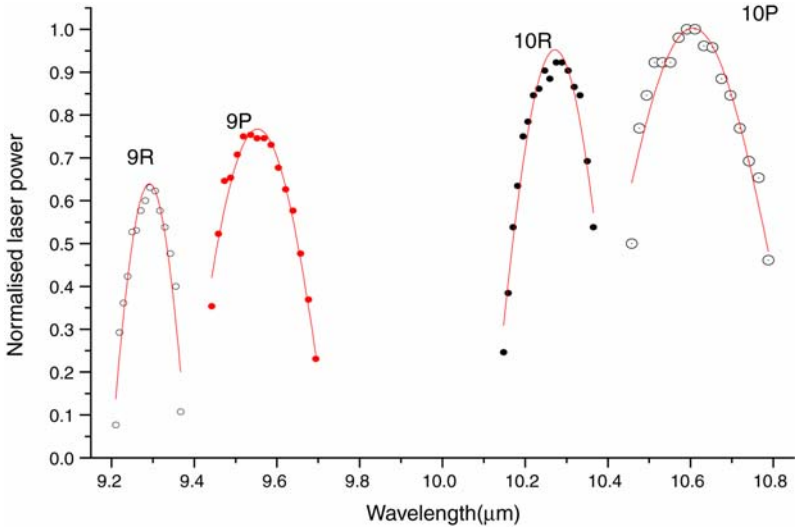

Note: The 10P(20) line showed the highest output power of roughly 50 W.

Figure 5 Change in laser beam radius and power density as the laser propagates after the focusing element

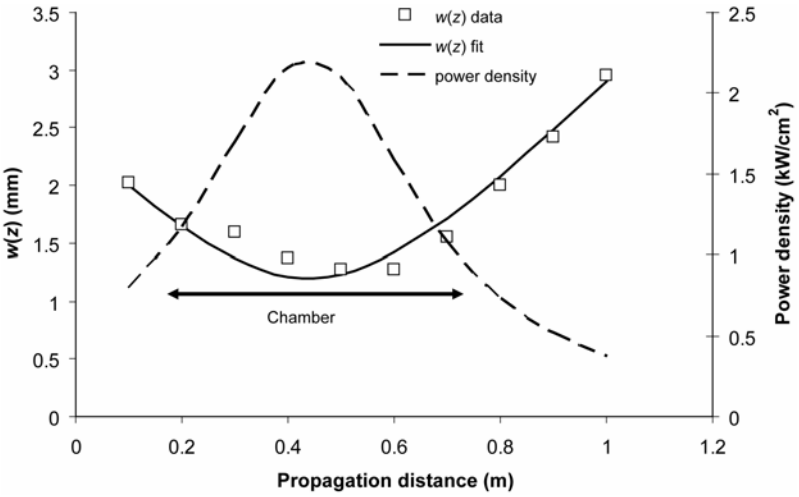

Note: The pyrolysis chamber was placed centred with the laser beam waist position, and is depicted in length on the plot. The power density reaches in excess of 2 kW/cm^2 at its most intense position.

Table 1 Important laser parameters for the pyrolysis experiment; some are measured directly while others are calculated from experimental data using the relations in Section 2

Propagation parameters			*Wavelength*	*Interaction volume*	*Power/power density*		
w_0	z_0	M^2	λ	V	P_0	$Max\ P_{peak}$	$Min\ P_{peak}$
1.2 mm	440 mm	1.68	10.6 μm	4 cm^3	50 W	2.2 kW/cm^2	0.9 kW/cm^2

We have noted a general lack of detail in the literature on full laser propagation parameters used in such experiments, with most authors concentrating only on the total power delivered. We point out here that since laser pyrolysis processes follow non-linear like responses to laser intensity (El-Diasty, 2004), it is imperative that all parameters relevant to calculating these intensities inside the reactor should be reported (such as those reported in Table 1). By not doing so, direct comparison of results becomes difficult to impossible, as is reproducibility. In addition, the laser beam's intensity distribution will also play an important role in the process (Forbes and Botha, 2005) and should where possible be reported. For example, multimode laser output will result in an ever changing intensity distribution due to propagation alone, whereas a Gaussian-like beam will remain Gaussian during free-space propagation. On the contrary, it has been shown (Forbes, 2006) that multimode like beams may in fact maintain their intensity distribution if the medium is suitably non-linear, as it most likely is in laser pyrolysis experiments (El-Diasty, 2004). Thus the laser beam parameters, such as spatial intensity distribution, beam quality and beam waist need to be reported, as they have been here.

Raman studies on the synthesised samples showed (see Figure 6(a)) two peaks near 700 cm^{-1} and 960 cm^{-1}, assigned to the O–W–O bending mode and W=O stretching mode, respectively (Grabrusenoks et al., 2001), but an absence of the characteristic peak at 804 cm^{-1} assigned to the O–W–O stretching mode of WO_3 (Lee et al., 1999). This signature is not consistent with that expected from the stoichiometry of WO_3, but rather is similar to that of W_3O_7 (Salje, 1977). After annealing an intense characteristic peak at 800 cm^{-1} appears as can be seen in Figure 6(b), indicating that WO_3 is formed. The Raman spectra do not change with the addition of O_2 or C_2H_2, indicating that these gases do not contribute to the dissociation process, as suspected. A SEM micrograph of the annealed samples at 5000 × magnification is shown in Figure 7(a), with the preannealed sample micrograph shown as an insert in the top left corner. The spherical particles before annealing are not clearly visible but after annealing almost perfectly spherical microsized particles of WO_3 are accompanied with very interesting additional nanosized features in the form of extended rods. Close examination of the microsizes spheres suggests that they are actually composed of smaller spheres in the nanosize scale; this might play an important role regarding the thermochromic and electrochromic properties of the material. A SEM micrograph of the annealed samples at 20,000 × magnification is shown in Figure 7(b), showing that rod-like nano structures are emanating from the sphere-like WO_3 structures. These rod-like nano structures are distinct entities with very little to no agglomeration. Image Tool™ image analysis software was used to analyse the surface morphology of the SEM images for size distribution of the rod-like nano structures formed. The size distribution charts, shown in Figure 8, indicated that the mean diameter of the rod-like structures was 51 nm, with a

mean length of 6.8 μm. We propose here that most (if not all) of these nano structures are in fact WO_3 nano-rods, which we base on the following argument:

1 Gillet et al. (2005) have observed that WO_3 nano-rods can be formed when potassium is present during the annealing process to act as a catalyst. We observe the presence of potassium through EDX analysis of the samples both before and after annealing (see Figure 9), and it is known that this is an impurity in the glass substrate

2 Our SEM images (Figure 7(b)) show clearly that the nanosized structures are emanating from microsized spheres (actually growing out of the structures), which we know to be WO_3 from Raman analysis.

These two facts lead us to conclude that the nano structures are in fact WO_3 nano-rods, formed for the first time during a laser pyrolysis process.

Figure 6 Raman spectra of tungsten oxides synthesised under oxygen and C_2H_2 conditions with: (a) as deposited and (b) after annealing at 500°C for 17 hr in argon (see online version for colours)

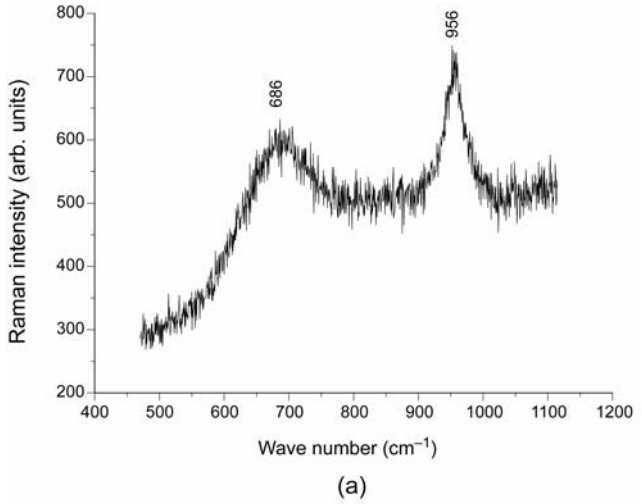

Figure 7 (a) SEM micrographs of a WO_3 sample prepared with the laser pyrolysis method. and (b) a close up on some of the nano-rods showing the emergence of the rod from the large spheres (see online version for colours)

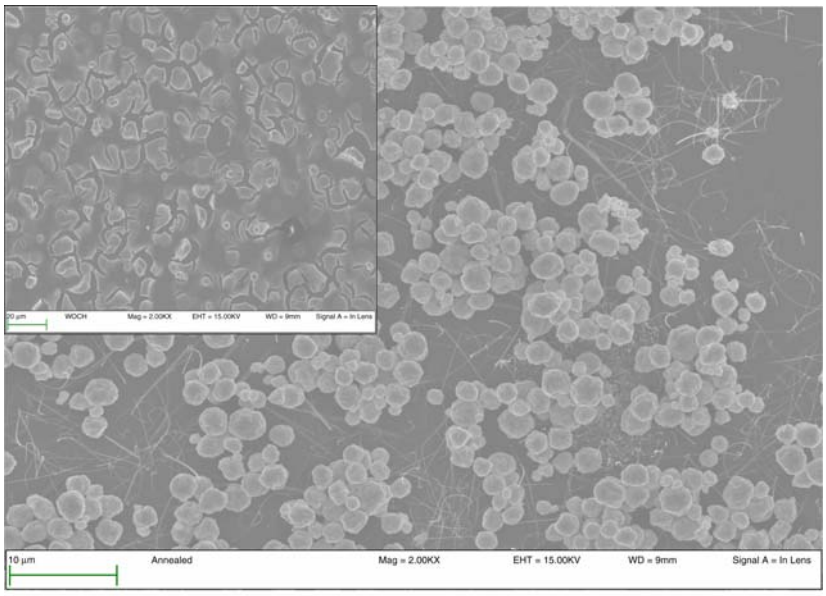

(a)

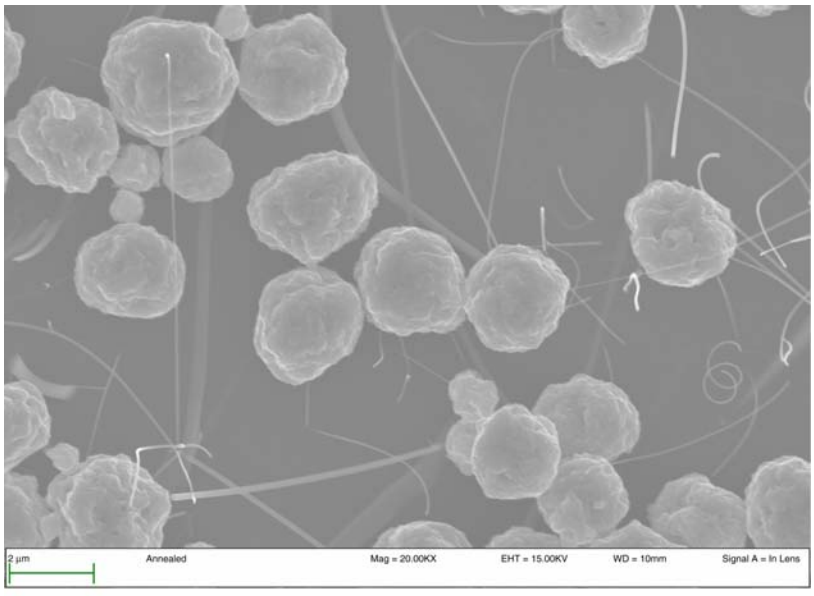

(b)

Note: The insert shows the sample prior to annealing while the larger image shows the same sample after annealing. The morphology change is clearly apparent, with tungsten oxide nano-wires in the background of the almost uniformly spherical particles of WO_3.

It also appears that some of these nano structures might be tubular in nature; this has yet to be confirmed by transmission electron microscopy.

Figure 8 Histograms of the diameter and length of a selection of the nanostructures shown in Figure 7

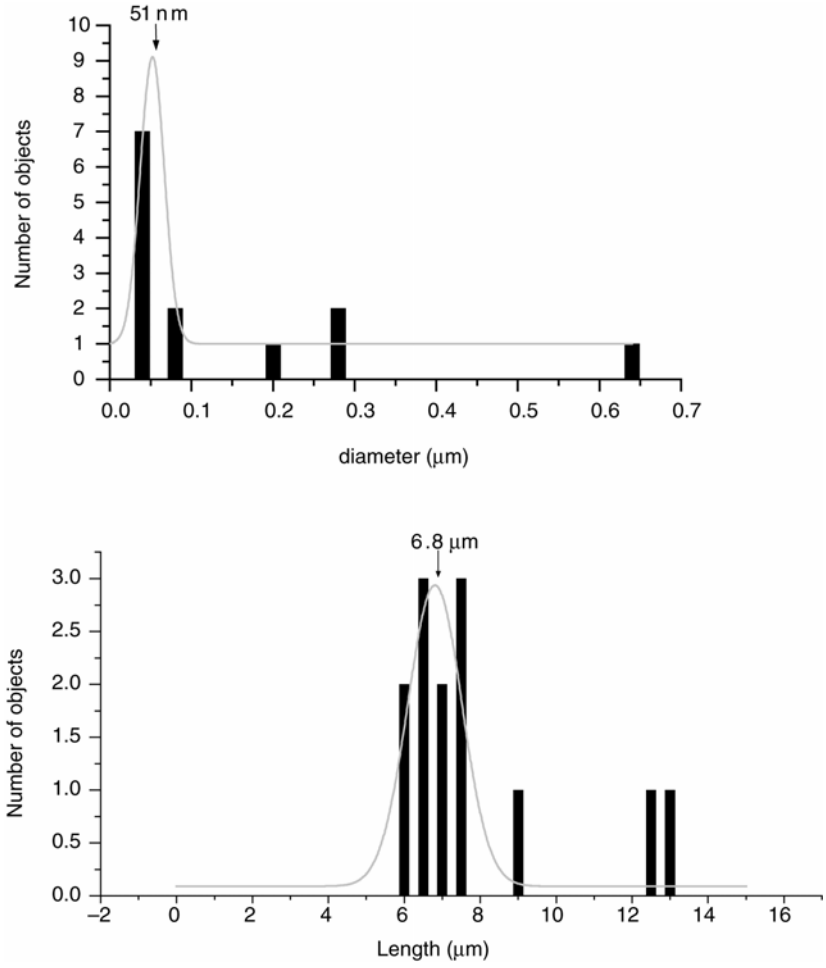

Note: The mean diameter and length of the WO_3 nano-rods (as determined from the fits) are 51 nm and 6.8 μm, respectively.

Finally we point out that the nanograins, although not having the desirable size necessary for affecting positively the thermo/electrochromic properties of WO_3, were produced without the flame contributing component (mixture of O_2 and C_2H_2) common in such experiments. This was a deliberate attempt at providing an environment for multiphoton dissociation only, with resulting reactions. Despite this nanosize spheres (around 200 nm diameter) formed an agglomeration leading to microsize particles. Since the results with only O_2 or C_2H_2 are identical and given that with only one of these gases present one does not produce a flame, we also propose that in this case the production of such nano structures is owing to the selective dissociation of the O–C bonds in the tungsten ethoxide precursor liquid, which is close to resonance with the 10.6 μm emission wavelength of the CO_2 laser employed. This 'first observation' report will in due course be followed with a more detailed study on the formation and properties of these structures.

Figure 9 EDX spectra for WO_3 samples (a) before annealing and (b) after annealing, showing the presence of the catalytic potassium (K) in both cases

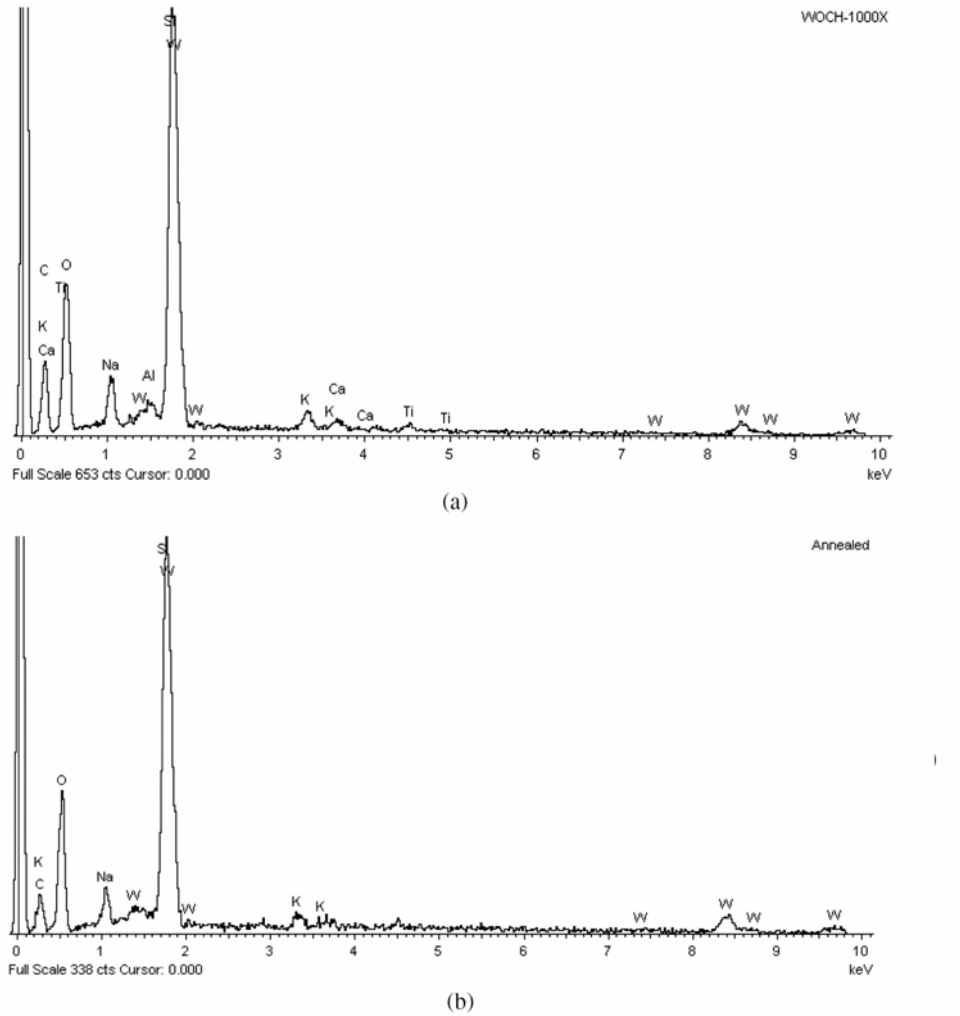

5 Summary

The synthesis of nanograin tungsten trioxide thin films for the first time by laser pyrolysis has been reported. A detailed description of the experimental set up has been outlined, and the need to present detailed information on the laser beam characteristics for comparison and repeatability of results has been highlighted. Investigation of the so-produced WO_3 thin films by Raman, EDX and by SEM was conducted and the results have been presented and discussed. The well-known Raman band at 800 cm^{-1} observed in all samples confirms the presence of WO_3 as agglomeration of nanosize particles. The present study also reports for the first time the presence of WO_3 nano-rods from laser pyrolysis. The fact that these structures appear in the presence of potassium seems to add weight to a previous proposal (Gillet et al., 2005) that potassium acts as a catalyst for the

formation of WO_3 nano-rods. The preliminary results from this study have shown that laser pyrolysis has great potential as a tool for fabricating nano-rods of high quality, given the straightness and lengthy nature of most of these nano-rods.

Acknowledgements

Sponsorship from the South African National Research Foundation (NRF) through project numbers: LREG 0001 and User Facility of the CSIR National Laser Centre of South Africa are greatly appreciated. We also acknowledge partial support of the Japanese Government through the Joint Japan/World Bank Graduate Scholarship Programme.

References

Amara, M., Hourlier, D. and El Ganaoui, M. (2003) 'A CFX-based model for Si/C/N ceramic nanopowder synthesis by laser pyrolysis', *3rd International Conference on CFD in the Minerals and Process Industries CSIRO*, Melbourne, Australia, pp.241–245.

Ando, M., Chabicovsky, R. and Haruta, M. (2001) 'Optical hydrogen sensitivity of noble metal-tungsten oxide composite films prepared by sputtering deposition', *Sensors and Actuators B*, Vol. 76, pp.13–17.

Arakaki, J., Reyes, R., Horn, M. and Estrada,W. (1995) 'Electrochromism in NiO_x and WO_x obtained by spray pyrolysis', *Solar Energy Materials and Solar Cells*, Vol. 37, pp.33–41.

Baraton, M.I., Merhari, L., Ferkel, H. and Castagnet, J.F. (2002) 'Comparison of the gas sensing properties of tin, indium and tungsten oxides nanopowders: carbon monoxide and oxygen detection', *Materials Science and Engineering C*, Vol. 19, pp.315–321.

Belanger, P.A. (1991) 'Beam propagation and the ABCD ray matrices', *Optics Letters*, Vol. 16, No. 4, p.196–198.

Bowden, C.M., Stettler, J.D. and Witriol, N.M. (1977) 'An excitation model for laser-induced photochemical reactions', *Journal of Physics B: Atomic and Molecular Physics*, Vol. 34, pp.1045–1050.

Cannon, W.R., Danforth, S.C., Flint, J.H., Haggerty, J.S. and Marra, R.A. (1982) 'Sinterable ceramic powders from laser-driven reactions', *Journal of the American Ceramic Society*, Vol. 65, pp.324–330.

Capanoe, S., Rella, R., Siciliano, P. and Vasanelli, L. (1999) 'A comparison between V_2O_5 and WO_3 thin films as sensitive elements for NO detection', *Thin Solid Films*, Vol. 350, pp.264–268.

Chapple, P.B. (1994) 'Beam waist and M^2 measurement using a finite slit', *Optical Engineering*, Vol. 33, No. 7, pp.2461–2466.

Dez, R., Porterat, D. and Boime, H. (2004) 'Silicon carbonitride nanopowders by laser pyrolysis for plastic nanocomposites', *Engineering Materials*, Vols. 264–268, pp.25–28.

Djerad, S., Tifouti, L., Crocoll, M. and Wesweiler, W. (2004) 'Effect of vanadia and tungsten loadings on the physical and chemical characteristics of V_2O_5-WO_3/TiO_2 catalysts', *Journal of Molecular Catalysis A: Chemical*, Vol. 208, pp.257–265.

El-Diasty, F. (2004) 'Simulation of CO_2 laser pyrolysis during preparation of SiC nanopowders', *Optics Communication*, Vol. 241, pp.121–135.

Forbes, A. (2006) 'Laser beam propagation in non-linearly absorbing media', *Proceedings of SPIE*, Vol. 6290, pp.31–37.

Forbes, A. and Botha, L.R. (2005) 'Isotope separation with infrared laser beams', in F.M. Dickey, S.C. Holswade and D.L. Shealy (Eds). *Laser Beam Shaping Applications*, Chapter 5, New York: CRC Taylor & Francis, pp.183–209.

Forbes, A., Strydom, H.J., Botha, L.R. and Ronander, E. (2002) 'Beam delivery for stable isotope separation', *Proceedings of SPIE*, Vol. 4770, pp.13–27.

Gillet, M., Delamare, R. and Gillet, E. (2005) 'Growth of epitaxial tungsten oxide nanorods', *Journal of Crystal Growth*, Vol. 279, pp.93–99.

Grabrusenoks, J., Veispals, A., von Czarnowski, P. and Meiwes-Broer, K.H. (2001) 'Raman and infrared characterization of tungsten trioxide', *Electrochimica Acta*, Vol. 46, p.2229–2231.

Haggerty, J.S. and Cannon, W.R. (1981) 'Sinterable powders from laser-driven reactions in laser-induced chemical processes', in J.I. Steinfeld (Ed). *Laser Induced Chemical Processes*, New York: Plenum Press, pp.105–121.

Herlin, N., Musset, A.X., Martinengo, M., Luce, H. and Cauchetier, M. (1996) 'Nanometric Si-based oxide powders: synthesis by laser pyrolysis and characterisation', *Journal of the European Ceramic Society*, Vol. 16, pp.1063–1073.

Hoel, A., Reyes, L.F., Heszler, P., Lantto, V. and Granqvist, C.G. (2004) 'Nanomaterials for environmental applications: novel WO3-based gas sensors made by advanced gas deposition', *Current Applied Physics*, Vol. 105, pp.283–289.

Huisken, F., Hofmeister, H., Kohn, B., Laguna, M.A. and Pillard, V. (2000) 'Laser production and deposition of light-emitting silicon nanoparticles', *Applied Surface Science*, Vols. 154–155, pp.305–313.

Jayatissa, A.H., Cheng, S.H. and Gupta, T. (2004) 'Annealing effect on the formation of nanocrystals in thermally evaporated tungsten oxide thin films', *Materials Science and Engineering B*, Vol. 109, pp.283–289.

Kamal, H., Akl, A.A. and Abdel-Hady, K. (2005) 'Influence of proton insertion on the conductivity, structural and optical properties of amorphous and crystalline electrochromic WO_3 films', *Physica B: Condensed Matter*, Vol. 349, pp.192–205.

Kawasaki, H., Namba, J., Iwatsuji, K., Suda, Y., Wada, K., Ebihara, K. and Ohshima, T. (2002) 'NO_x gas sensing properties of tungsten oxide thin films synthesised by pulsed laser deposition method', *Applied Surface Science*, Vols. 197–198, pp.547–551.

Lee, S.H., Cheong, H.M., Tracy, C.E., Mascarenhas, A., Benson, D.K. and Deb, S.K. (1999) 'Effects of W valency on Raman', *Electrochimica Acta*, Vol. 44, pp.3111–3115.

Leftheriotis, G., Papaefthimiou, S., Tianoulis, P., Siokou, A. and Kefalas, D. (2003) 'Structural and electrochemical properties of opaque sol-gel deposited WO3 layers', *Applied Surface Science*, Vol. 218, pp.275–280.

Muller, A., Herlin-Boime, N., Tenegal, F., Berger, A.X., Flank, A.M., Romuald, D., Muller, K., Bill, J. and Aldinger, F. (2003) 'Comparison of Si/C/N pre-ceramics obtained by laser pyrolysis or furnace thermolysis', *Journal of the European Ceramic Society*, Vol. 23, pp.37–46.

Mwakikunga, B.W., Sideras-Haddad, E. and Maaza, M. (2007) 'First synthesis of vanadium dioxide by ultrasonic nebula-spray pyrolysis', *Optical Materials*, Vol. 29, pp.481–487.

Patil, P.R. and Patil, P.S. (2001) 'Preparation of mixed oxide MoO_3-WO_3 thin films by spray pyrolysis technique and their characterisation', *Thin Solid Films*, Vol. 382, pp.13–22.

Patil, P.S., Nikam, S.B. and Kadam, L.D. (2001) 'Influence of substrate temperature on the properties of sprayed WO_3 thin films', *Materials Chemistry and Physics*, Vol. 69, pp.77–83.

Petcu, S., Cauchetier, M., Armand, X., Voicu, I. and Alexandrescu, R. (2000) 'Formation of fullerenes in laser pyrolysis of benzene', *Combustion and Flame*, Vol. 122, pp.500–507.

Pola, J., Pokorna, D., Bohacek, J., Bastl, Z. and Ouchi, A. (2004) 'Nano-structured crystalline Te films by laser gas-phase pyrolysis of dimethyl tellurium', *Journal of Analytical and Applied Pyrolysis*, Vol. 71, pp.739–746.

Salje, E. (1977) 'Normal WO_3 crystal vibration modes', *Acta Crystallographica B*, Vol. 33, pp.574–577.

Shieh, J., Feng, H.M., Hon, M.H. and Juang, H.Y. (2002) 'WO_3 and W-Ti-O thin film gas sensors prepared by sol-gel dip- coating', *Sensors and Actuators B*, Vol. 86, pp.75–80.

Siegman, A.E. (1991) 'Defining the effective radius of curvature for a nonideal optical beam', *IEEE Journal of Quantum Electronics*, Vol. 27, No. 5, pp.1146–1148.

Siegman, A.E. and Townsend, S.W. (1993) 'Output beam propagation and beam quality from a multimode stable-cavity laser', *IEEE Journal of Quantum Electronics*, Vol. 29, No. 4, pp.1212–1217.

Sun, Q., Rao, B.K., Jena, P., Stolcic, D., Gantefor, G. and Kawazoe, Y. (2004) 'Effect of sequential oxidation on the electronic structure of tungsten clusters', *Chemical Physics Letters*, Vol. 387, pp.29–34.

Tenegal, F., Petcu, S., Herlin-Boime, N., Armand, X., Mayne, M. and Reynaud, C. (2001) 'Effect of the C/O ratio on the C_{60} and C_{70} formation rates in soot synthesised by laser pyrolysis of benzene-based mixtures', *Chemical Physics Letters*, Vol. 335, pp.155–162.

van Erven, W.J.M., Trzeciak, T.M., Fu, Z. and Marijnissen, J.C.M. (1997) 'Design of a laser assisted aerosol reactor for production of ceramics on a semi-industrial scale', *Journal of the European Ceramic Society*, Vol. 17, pp.1045–1052.

Wang, S.H., Chou, T.C. and Liu, C.C. (2003) 'Nano-crystalline tungsten oxide NO_2 sensor', *Sensors and Actuators B*, Vol. 94, pp.343–351.

Watanabe, A., Unno, M., Hojo, F. and Miwa, T. (2003) 'Silicon-germanium alloy prepared by laser-induced pyrolysis of organo-germanium nanocluster spin-coated on Si substrates', *Materials Letters*, Vol. 57, pp.3043–3047.

Wright, D., Greve, P., Fleischer, L. and Austin, L. (1992) 'Laser beam width, divergence and beam propagation factor: an international standardization approach', *Optical and Quantum Electronics*, Vol. 24, pp.S993–S1000.